Mon. Not. R. Astron. Soc. **276**, 689–705 (1995)

A study of the large-scale distribution of galaxies in the South Galactic Pole region – I. The data★

S. Ettori,[1,2] L. Guzzo[1] and M. Tarenghi[2]

[1] *Osservatorio Astronomico di Brera, Via Bianchi 46, I-22055 Merate (CO), Italy*

[2] *European Southern Observatory, K. Schwarzschild Str. 2, D-85748 Garching, Germany*

Accepted 1995 April 3. Received 1995 March 24; in original form 1994 August 22

ABSTRACT

We present the data from an extensive, moderately deep ($b_J \sim 19.5$) spectroscopic survey of ~600 galaxies within four regions of sky located near the South Galactic Pole. About 75 per cent of the measured galaxies are in an approximately $3° \times 1.5°$ region dominated by the rich cluster of galaxies Klemola 44 (Abell 4038). The other three smaller areas cover about 1 deg^2 each. Here, we discuss in detail the observing and data reduction strategies, and the completeness of and errors in the measured redshifts. The data collected are being used for: (i) a study of the large-scale redshift distribution of the galaxies in each field, and (ii) a thorough dynamical investigation of Klemola 44. Results from these analyses will be presented in forthcoming papers.

Key words: surveys – galaxies: general – large-scale structure of Universe.

1 INTRODUCTION

During the 1980s the industry of redshift measurements produced some of the most remarkable results on the large-scale structure of the Universe. In particular, the CfA survey (Huchra et al. 1983; Geller & Huchra 1989), and the Perseus–Pisces survey (Giovanelli, Haynes & Chincarini 1986), covered wide solid angles on the sky, measuring redshifts for complete magnitude-limited subsamples of the Zwicky et al. (1963–68) catalogue. These, and other subsequent surveys (see Giovanelli & Haynes 1991 for a review), were all performed with single object spectroscopy, i.e. measuring one spectrum at a time. While the first multi-object spectrographs were being developed during the first half of the decade (Gray 1984; see in particular the two excellent reviews by Ellis & Parry 1988, and Hill 1988), the typical surface density of objects at the limiting magnitudes reached by the available catalogues ($m_b \leq 15.5$) was simply too low by a factor of 100 or more for justifying, or even vaguely suggesting, the use of multiplexing in large-scale redshift survey work. To our knowledge, the first use of a multi-object spectrograph for extensive galaxy redshift survey work, although still limited to small fields, was the faint galaxy survey of Broadhurst, Ellis & Shanks (1988) using the FOCAP fibre coupler at the Anglo–Australian Telescope (AAT).

★Based on data collected at the European Southern Observatory, La Silla, Chile.

In 1987 we became aware of the ongoing activity in the UK to construct two large digitized catalogues of galaxies, the Edinburgh/Durham Southern Galaxy Catalogue (EDSGC: Heydon-Dumbleton, Collins & MacGillivray 1989) and the APM catalogue (Maddox, Efstathiou & Sutherland 1990), starting from the same photographic material, i.e. the ESO/SRC J plates. Given their faint limiting magnitude ($b_J \sim 20.5$), these catalogues represented an ideal data base for conceiving a further step in redshift survey work, i.e. using a wide-field multi-object spectrograph for surveying in depth a large area of the sky. For these reasons, in 1988 we started a preliminary program aimed to test the performances of what, at the time, was a new prototype version of the ESO fibre spectrograph OPTOPUS (Avila et al. 1989). The idea was eventually to start at ESO a dedicated program of large-scale redshift survey down to $b_J \sim 19$–19.5, the magnitude that optimizes the use of the instrument by matching the number of available fibres (Guzzo & Tarenghi 1987). Here we present the data from this early test survey over four selected regions of sky, which fully confirmed the reliability of OPTOPUS for such a project (see Avila et al. 1989). Eventually, a complete large-scale redshift survey based on the EDSGC to the same limiting magnitude, over a strip of $\sim 30° \times 1°$, was started in 1991 and is presently under completion (ESO Slice Project, hereafter ESP, Vettolani et al. 1994).

Forthcoming papers related to the data presented here will discuss the large-scale galaxy distribution in depth, and the kinematics of the cluster Klemola 44/Abell 4038 (Klemola 1969).

2 THE SURVEY

2.1 Sample selection

In the planning of a large redshift survey, a basic starting point is represented by the availability of a photometric catalogue of galaxies complete to some limiting magnitude. A notable example of this sense has been represented by the Zwicky et al. (1963–68) Catalogue of Galaxies and Clusters of Galaxies (CGCG), which has been used for a number of redshift surveys of optical galaxies (see Oort 1983; Rood 1988; Giovanelli & Haynes 1991, and references therein). At the end of the eighties, however, a major step forward in this field has been achieved through the construction of two large automatic catalogues of galaxies, already mentioned in the introduction, the EDSGC (Heydon-Dumbleton et al. 1989) and the APM catalogue (Maddox et al. 1990). Both of these compilations were constructed by digitizing the plates of the ESO/SRC J photographic survey, and then analysing the digital data to separate stars from galaxies. Star/galaxy separation is accomplished to better than ~5 per cent accuracy, and the catalogues are fairly complete to a magnitude $b_J = 20.5$. Since initially these catalogues were constructed with a view to using them for cosmological studies, particular care was devoted to the plate-to-plate matching of the internal magnitude system, to avoid the possibility of spurious calibration inhomogeneities mimicking large-scale clustering.

The availability to us of parts of the EDSGC since its early stages of construction represented the driving force that stimulated the observations presented in this paper. The EDSGC has been put together starting from the survey plate scans performed in Edinburgh using the COSMOS machine (Beard, MacGillivray & Thanisch 1990), which provides a relative positional accuracy ~0.5 arcsec (over small areas). This is ideally suited to use with an optical fibre spectrograph, where light is collected over apertures of 1–2 arcsec diameter (see next section). In addition, the faint magnitude reached by these catalogues allows us to match easily the density of fibres on the spectrograph. In the case of the 33 arcmin field of OPTOPUS, the fibre spectrograph used here, the match with the average galaxy number counts in the b_J band is for $b_J \simeq 19.2$–19.5.

As discussed in the introduction, the observations presented here were mostly intended as preliminary tests of the performances of the upgraded version of the ESO fibre spectrograph OPTOPUS when used for medium–deep redshift survey work. We already had at our disposal from previous observations ~170 unpublished redshifts in the area of the cluster Klemola 44 (K44 hereafter), near the South Galactic Pole. Our effort was concentrated in trying to collect a large quantity of radial velocities for galaxies in this same area, which we named PL, to allow a very detailed kinematical study of the cluster. This area was covered with a mosaic of 18 OPTOPUS fields, some of which had to be observed twice given the large number of objects with respect to the average number counts. The honeycomb geometry of the mosaic is shown in Fig. 1(a). In addition to this region, we observed another two smaller areas east and west of K44, called respectively PW and FD. These were meant to provide in-depth clustering information in areas not dominated by a single conspicuous cluster, with the practical benefit of allowing a more homogenous right ascension coverage during the night. Figs 1(b) and (c) show the disposition of the OPTOPUS fields in these areas. A fourth region, PE, was also partly covered during the observations (Fig. 1d), but due to bad weather conditions only a few redshifts in two OPTOPUS fields were obtained. These are also presented here, but are evidently too scarce to allow any possible use of the PE region in the parallel analyses we are performing (Ettori et al. 1995a,b, in preparation). Table 1 gives the central coordinates of the single OPTOPUS fields observed. Fig. 2 gives an all-sky view of the positions of the observed fields, indicating also for comparison the region covered by the EDSGC, the position of the famous NGP–SGP pencil-beam of the faint galaxy survey of Broadhurst et al. (1990; hereafter BEKS), and the area covered by the ESP survey.

2.2 Observations

OPTOPUS is a fibre-optic coupling system developed for the Cassegrain focus of the ESO 3.6-m telescope, which allows multi-object spectroscopy within a field of 33 arcmin diameter. Aluminium starplates with fibre holders have to be prepared in advance of the observation. These are eventually mounted at the telescope and the fibres are manually inserted into the apertures. At their opposite end, the fibres form the entrance slit of the spectrograph. In its original version, before 1988, the system suffered from poor throughput of the fibres, mainly due to the presence in front of each fibre of a microlens used to convert the focal ratio from the $f/8$ output of the Cassegrain focus to $f/3$ (Lund & Enard 1984). In the new version, which was tested for the first time during our observations, new Polymicro fibres with reduced focal-ratio degradation and enhanced blue–UV transmission, are placed directly in the focal plane of the telescope. The new fibres allow direct coupling to the $f/8$ collimator of a Boller & Chivens spectrograph. The global improvement in efficiency of the new configuration has been evaluated to be about one magnitude (Avila et al. 1989).

For our program, the ESO grating number 15 was used together with the $f/8$ collimator and $f/1.9$ blue camera of the B&C spectrograph. This configuration gives a dispersion of 170 Å mm^{-1} and a FWHM resolution of about 10 Å. For studies of the large-scale distribution of galaxies it is necessary to keep the error on the measured redshifts below 100 km s^{-1}. The use of the cross-correlation technique for the redshift estimate allows rms errors between 1/25 and 1/10 of the nominal, single-line resolution, to be reached, depending on the S/N ratio of the spectrum. The expected uncertainty on cz, given our spectroscopic setup, was then between 25 and 60 km s^{-1}. As we shall see, this is well matched by the actual errors estimated on the measurements.

The observations were performed during seven nights in 1988 August/September and four nights in 1989 October. During the 1988 run, 2.5 nights were lost due to bad weather; in 4.5 nights of actual observations, 21 independent OPTOPUS fields were observed. The success rate related to bad weather or technical problems, for the 1989 run, was around 80 per cent, with 17 fields observed. Some of these were re-observations of some of the PL fields, to increase their completeness. The total number of independent fields in the whole survey on which at least one redshift was obtained is 30, as also shown by Fig. 1.

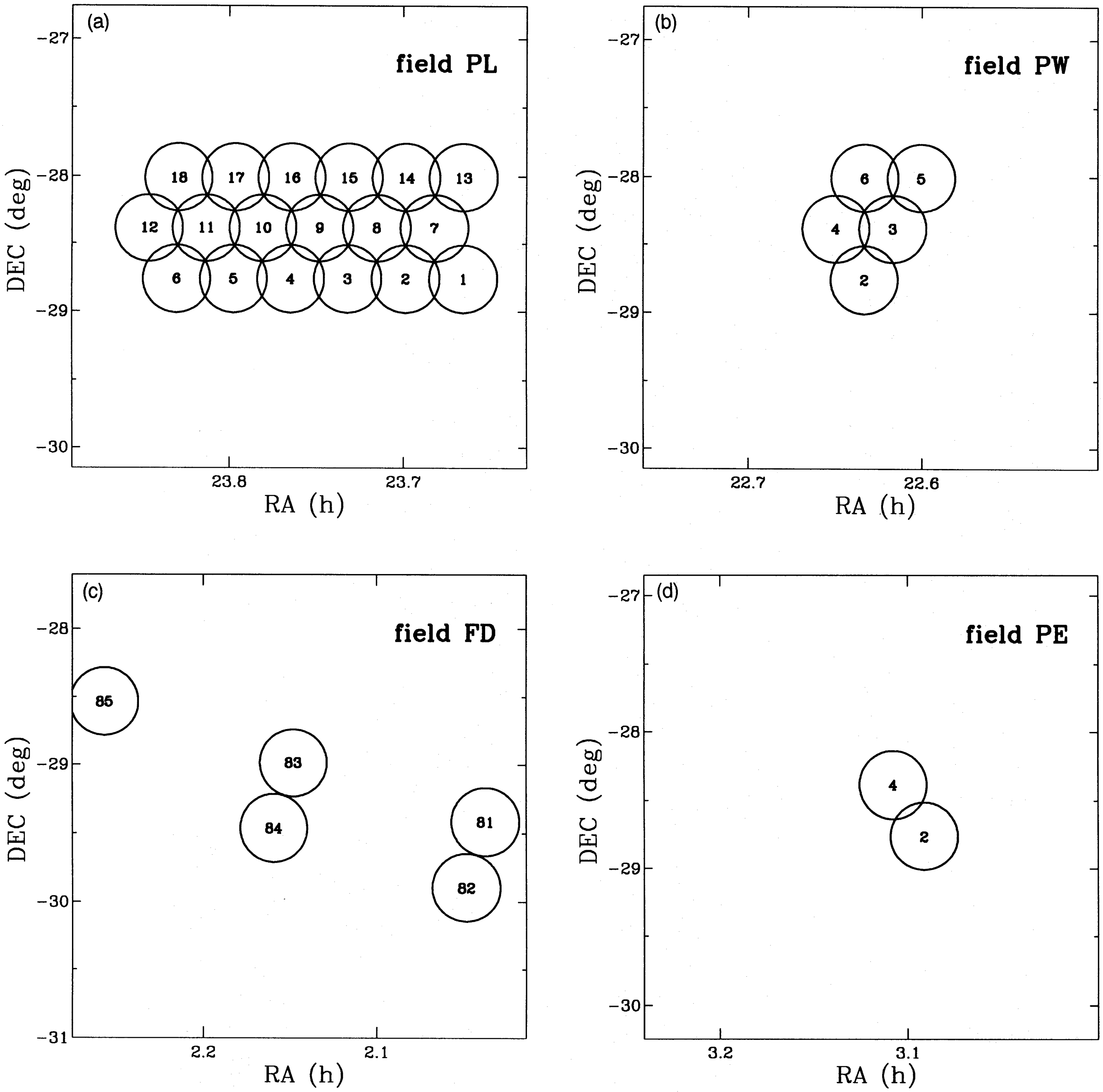

Figure 1. (a, b, c and d) Geometrical configuration of the observed 33 arcmin OPTOPUS fields. With the exception of the FD region, the galaxies were selected to lie within adjacent hexagons constructed within each OPTOPUS field. This honeycomb geometry is the simplest way to fully cover an area of the sky using a circular field instrument.

Total exposure times were between 60 and 90 min, typically divided into two–three exposures aimed at allowing accurate cosmic-ray elimination. Three to four fibres were used during each exposure to collect the sky spectrum. He–Ar calibration spectra were observed immediately before and after the science exposures, through the same fibre configuration and with the telescope in the same position, as well as quick lamp flat-field frames. Standard bias frames were taken in multiple exposures at the beginning and end of each night.

3 DATA REDUCTION AND REDSHIFT DETERMINATION

3.1 Standard reduction and wavelength calibration

All the data were reduced using the IRAF package running on a SUN SparcStation II at the Osservatorio Astronomico di Brera. After properly subtracting the bias – as obtained from several, median-averaged, single-bias exposures – and trimming the outer superfluous regions of the CCD frames, the 2–3 exposures available for each field were combined.

Table 1. The coordinates (1950) of the 31 Optopus fields observed.

field	RA	DEC
pw2	22:37:59	-28:45:41
pw3	22:37:00	-28:23:11
pw4	22:38:58	-28:23:11
pw5	22:36:01	-28:00:01
pw6	22:37:58	-28:00:01
pl1	23:39:57	-28:45:41
pl2	23:41:55	-28:45:41
pl3	23:43:54	-28:45:41
pl4	23:45:52	-28:45:41
pl5	23:47:51	-28:45:41
pl6	23:49:49	-28:45:41
pl7	23:40:56	-28:23:11
pl8	23:42:54	-28:23:11
pl9	23:44:52	-28:23:11
pl10	23:46:50	-28:23:11
pl11	23:48:48	-28:23:11
pl12	23:50:46	-28:23:11
pl13	23:39:57	-28:00:41
pl14	23:41:54	-28:00:41
pl15	23:43:52	-28:00:41
pl16	23:45:50	-28:00:41
pl17	23:47:47	-28:00:41
pl18	23:49:45	-28:00:41
fd81	2:02:18	-29:25:01
fd82	2:02:57	-29:53:48
fd83	2:08:53	-28:59:08
fd84	2:09:33	-29:27:48
fd85	2:15:24	-28:32:03
pe2	3:05:29	-28:45:41
pe4	3:06:28	-28:23:11

This was performed in general through a k–σ–clipping algorithm intended for eliminating cosmic ray (CR) events. The proper IRAF task was then used to extract the single spectra from the frames. The algorithm performs an optimal extraction, also following possible distortions of the spectra along the dispersion direction. It also allows rejection of discrepant pixels, as residual CR events which survived the initial cleaning phase. The extraction model profile was obtained from the high S/N ratio flat-field of each frame, and contemporarily to the science spectra, the corresponding He–Ar spectra were also extracted. The final result of this operation was represented by two sets of $n \leq 31$ one-dimensional spectra (objects plus arcs), for each observed field, ready for the subsequent wavelength calibration. To improve the stability of the wavelength calibration solution, in addition to the He–Ar lines we used the strong night-sky line O I λ5577 Å. The position of this sky line is particularly well suited to fill the gap existing in the He–Ar spectrum between 5100 and 5800 Å, where no bright enough line is present. The addition of the O I λ5577-Å line allowed us to work with a nice set of ~10 very good S/N lines, evenly distributed over the spectral range of interest, and obtain typical rms calibration errors of ~0.2 Å.

3.2 Sky subtraction

Sky subtraction for optical fibre data is typically not a straightforward task (see e.g. Ellis et al. 1984). In our case, we adopted the following strategy. During the observations, (typically) four fibres in each field were dedicated to collecting light from the night sky. The position of these fibres was fixed during the starplate preparation phase, and chosen to avoid cross-talk with the object fibres. As we shall see, in a

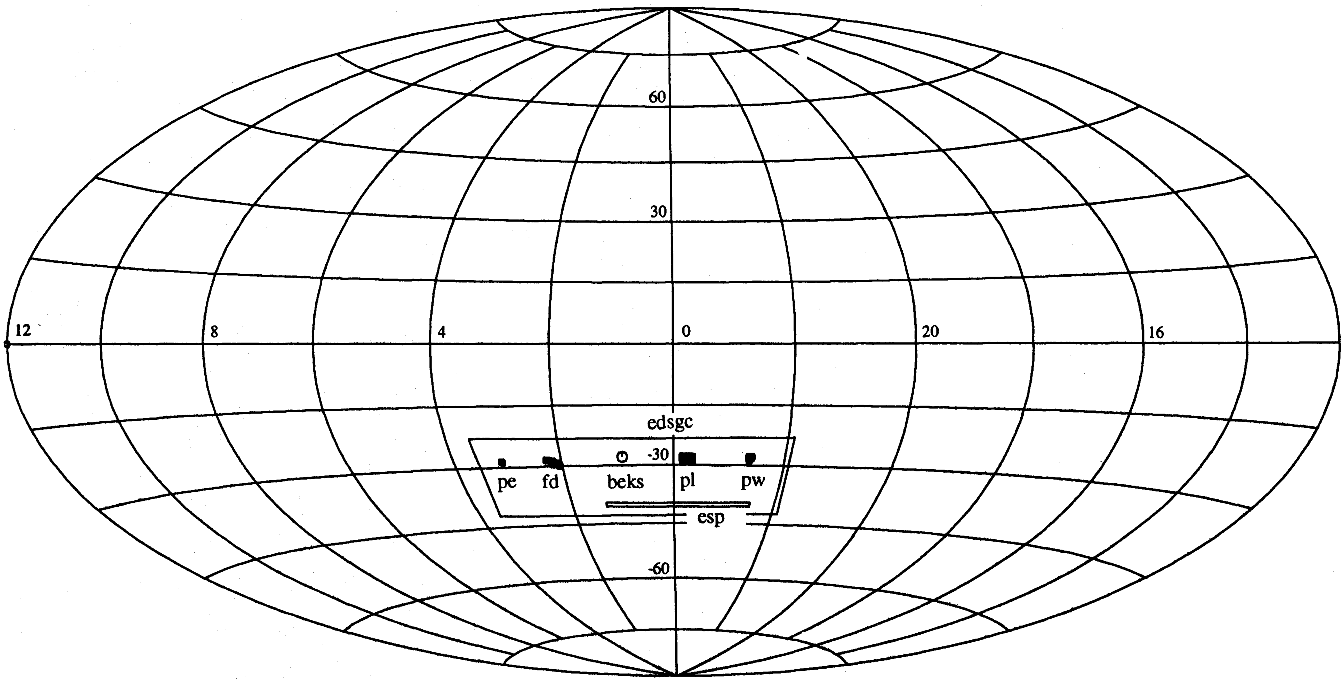

Figure 2. Aitoff all-sky projection showing the position of the observed fields on the celestial sphere, compared to that of the BEKS SGP beam (open circle). The largest (solid) rectangular region shows the area covered by the EDSGC (60 Schmidt plates), while the thin east–west strip is the area surveyed by the ESP project of Vettolani et al. (1994).

few cases a sky fibre was found to have collected light from an unexpected object, evidently fainter than the limit of the survey at $b_J = 19.5$, providing a redshift for an additional 'foreign' galaxy.

The main issue for achieving a sufficiently accurate sky subtraction is the normalization of the throughput of the single fibres to a common scale. The throughput is essentially independent of the wavelength, but is strongly related to the fibre bending and torsion, thus to the actual position of the telescope. One possibility for normalizing the relative transmission of the sky and object fibres is to use the continuum lamp flat-fields observed before and after each science exposure. However, we tried to use an even more direct method to measure the actual throughput based on the relative fluxes in the bright night-sky lines. We first developed an IRAF procedure which automatically measures the flux f in the two sky emission lines O I $\lambda\lambda$5577 and 6300 Å for all the spectra of the same OPTOPUS field. The program measures the ratio

$$r_f = \frac{f(\mathrm{O\,I}\,\lambda 5577\,\text{Å})}{f(\mathrm{O\,I}\,\lambda 6300\,\text{Å})},$$

and then calculates the mean and standard deviations of the distribution of r_f among the different spectra. The aim of this was to identify spectra for which the estimate of the flux in one or both of the sky lines used is corrupted by, e.g., the coincidence with a galaxy absorption or emission feature or with a residual CR spike. We defined therefore as 'good' those spectra with r_f values within $\langle r_f \rangle \pm \sigma_{r_f}$. Among these we chose as reference the spectrum with the highest O I λ5577-Å line flux, and normalized each spectrum by multiplying it by the ratio of its O I λ5577-Å line flux to the reference one. Spectra which had r_f outside of the $\pm 3\sigma$ interval around the mean were flagged and inspected. Typically, one of the two sky lines was affected by a feature in the galaxy spectrum. In this case, we used for the normalization the remaining 'good' line. The result of this operation was thus a set of 31 spectra, normalized to a common response curve, among which 3–4 were pure sky spectra.

The sky spectra were then averaged through a 3-σ-clipping average, constructing a mean sky spectrum which was subtracted from all object spectra belonging to the same field. The results were individually checked, and residuals from imperfectly subtracted bright sky lines were manually eliminated by interpolation of the adjacent continuum. A few examples of spectra of different quality are shown in Fig. 3.

3.3 Spectral templates

The basis of the cross-correlation technique for redshift measurement is the comparison of the object spectrum with a model spectrum of known radial velocity and ideally infinite S/N ratio: the *template.* The power of this technique lies in the remarkable similarity in the basic features among galaxy spectra, although the relative intensity of absorption lines can vary quite significantly, in particular when different morphological types are considered. In practice, to cover the range of spectral properties a number of different templates are used for each object, and the one producing the highest cross-correlation peak is then taken to be the best model, at zero radial velocity, of the galaxy spectrum being measured.

3.3.1 Internal stellar templates

In the present work particular care has been devoted to the definition, choice and – in some cases – construction of the template spectra. After the first set of observations was performed, it was clear that some of the stars misclassified as galaxies in the EDSGC (~5 per cent) and thus observed during the survey, were quite appropriate for use as stellar templates. This is the case for late G and K spectral types, i.e. those which represent the dominant contribution to the global galaxy spectrum. Having also at our disposal a library of galaxy and further stellar templates used for other projects (see below), no other template was specifically observed during the subsequent runs of the survey.

It is instructive to detail the procedure followed to select the best 'internal' templates (i.e. observed with the same instrumentation as the objects to be measured). We first inspected directly all the brightest stellar spectra among the available data, checking the prominence of the H_β λ4861 Å, Mg I λ5175 Å, Na I λ5892 Å lines, the G λ4304 Å and Ca + Fe λ5269 Å bands. In this way we selected a group of 60 G–K stars, potentially suited to use as templates. During the visual inspection of the spectra, we qualitatively divided them into five broad spectroscopic subgroups on the basis of similar intensity ratios among the above mentioned absorption features. This allowed us to construct five synthetic spectra by averaging, after weighting for the continuum intensity, the spectra in the five classes. Note that the spectra were combined without correcting their own heliocentric radial velocity, in an attempt to mimic the broadening effect produced by the stellar velocity dispersion on the galaxy spectrum absorption lines. Obviously, this is quite an arbitrary operation, and cannot be considered as an acceptable method for the proper construction of a synthetic galaxy spectrum starting from its basic stellar components. The only aim is to empirically improve the significance of the cross-correlation output, to be checked a posteriori on the actual results. In fact, the cross-correlation of the single spectra of each group among themselves showed a typical dispersion among the different stars ~50 km s^{-1}, i.e. of the order of the errors on each single cross-correlation measurement, but still smaller than typical internal velocity dispersions in galaxies. A direct cross-correlation test of the synthetic spectra on a set of science spectra showed that these were performing in a number of cases better (i.e. providing a more significant peak) than the single components.

The performances of the 60 single stellar template candidates were tested by applying them (after determining their zero-point velocity as described below), to estimate the redshift of three galaxies with accurately known radial velocity, for which we had high S/N spectra from a previous project (Collins et al. 1995): NGC 6070, 5746 and 5796. All of these galaxies have 21-cm line redshift measurements with error of <10 km s^{-1}. As a result, we selected the four best stellar templates on the basis of their ability to approach the 'true' redshift of the three galaxies with high significance.

In summary, at the end of this selection procedure we had at our disposal nine 'stellar' templates observed with the same identical instrumentation as the target galaxies of the survey, four single stars plus five synthetically combined spectra.

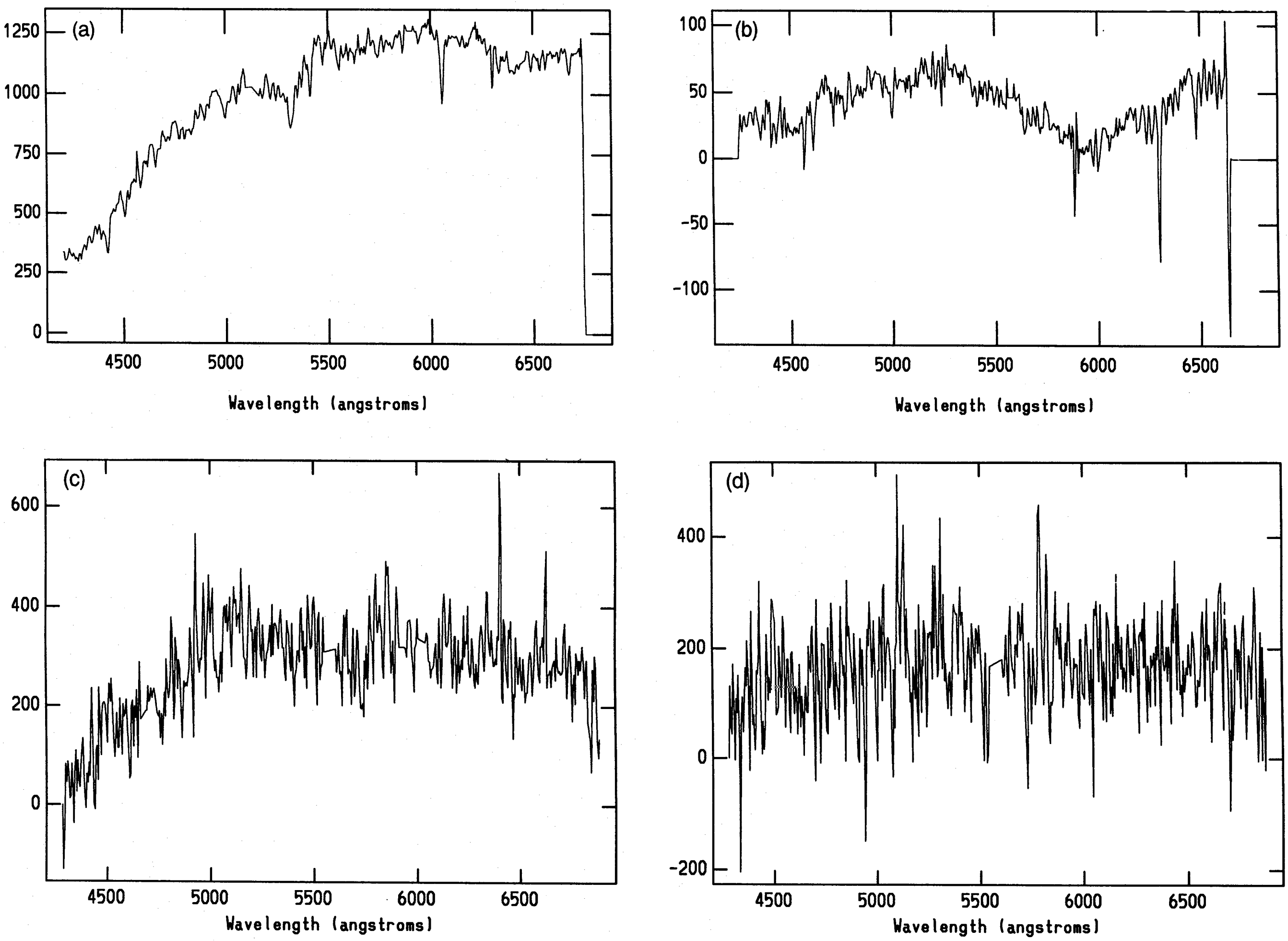

Figure 3. Some examples of spectra of different quality from the survey. Spectra are not flux-calibrated, thus the ordinates give only the relative intensity in arbitrary units. (a) Spectrum of a $b_J = 15.90$ galaxy (RA$= 23^h41^m34\overset{s}{.}1$, Dec.$= -28°34'35''$), which gave a redshift with very high confidence, $R = 19.3$. (b) Example of a spectrum that still gives a good confidence level ($R = 5.13$. RA$= 23^h44^m27\overset{s}{.}1$, Dec.$= -28°14'08''$, $b_J = 18.70$) despite having possibly undergone some problems during sky subtraction. (c) Example of a lower S/N spectrum (RA$= 02^h14^m35\overset{s}{.}3$, Dec.$= -28°30'48''$, $b_J = 18.91$), with $R = 3.90$, which is the median value of the distribution of R among the whole set of spectra. (d) Example of a very low S/N spectrum (RA$= 23^h43^m04\overset{s}{.}1$, Dec.$= -28°23'45''$, $b_J = 19.36$), which gave $R = 1.87$, the lowest value of R among the data included in the final table. Cases like this, i.e. below the exclusion threshold of $R = 3$, are passed only after positive visual inspection of the cross-correlation function. They have, in any case, to be considered as tentative.

3.3.2 *Internal galaxy templates*

After running a first test cross-correlation session over the whole set of spectra – as described below – we realized that some of the spectra of galaxies in the survey with particularly good S/N ratios consistently gave very significant cross-correlation peaks, with a confidence parameter (see below for definition), $R \sim 10$ or larger. In addition, we noted how the ability of the cross-correlation algorithm to efficiently detect redshifts larger than 10 000 km s^{-1} was clearly reduced by the fact that internal stellar templates have a starting wavelength ~4200 Å. In this way, important absorption features at lower wavelength, especially the CaK λ3934-Å and CaH λ3968-Å lines, are not present in the template spectrum. These absorption lines enter the observed wavelength range for objects with $cz > 20\,000$ km s^{-1}, and are therefore very useful for estimating the redshift of distant galaxies with typically faint spectra. It was therefore particularly important to include in the final set of templates a number of galaxies with high recession velocity, selected among those giving high values of R. In the attempt to cover a redshift range as wide as possible, we assembled the best galaxies of the survey, defined as having a best confidence parameter $R > 10$, into four broad distance classes, characterized respectively by $cz \sim 10\,000$, $\sim 20\,000$, $\sim 30\,000$ and $> 30\,000$ km s^{-1}. For each class, the object with the largest average R among the different templates was promoted as a new galaxy template. The average was performed excluding the best and the worst of the values of R obtained with the different templates, to enhance those spectra with the more general spectral features. The second-best R galaxy in the first class was also included in the selected set due to its high S/N ratio and particularly good performances with all of the templates.

In summary, this selection provided us with five further templates observed with the same identical instrumentation as the survey objects. The important feature of this new set is that they are galaxy spectra, with good blue coverage.

3.3.3 *Template zero point*

The above described operations produced a set of 14 internal templates: four stars, five composite stars and five galaxies. A crucial operation for minimizing the error on the redshift measurement is the determination of the radial velocity for each template, i.e. what will represent the zero points of our velocity measurements. To this end, we adopted a two-step procedure which can be described as follows. Andrew Connelly kindly provided us with a set of seven radial velocity Henry Draper (HD) standard stars, observed at the AAT telescope with moderately high resolution (1.4 Å pixel) and high S/N ratio, covering the wavelength range 3500–6500 Å. For these stars, a very accurate radial velocity is provided in the Astronomical Almanac, as detailed in Table 2. Our final goal was to use these (or some of these) higher precision templates as zero-point velocity calibrators for our internal set of templates. To this end, we had to be absolutely sure that the actual radial velocities of the HD spectra had errors consistent with those quoted in the Almanac. These spectra had nearly five times higher resolution than those in our survey, and could therefore provide a very tight constraint on the redshift of our internal templates (obviously within the intrinsic resolution of the latter ones). The only uncertainty about the HD radial velocities was the possibility of some systematic error in the spectra available to us, which could have introduced non-negligible shifts with respect to the published values. To ascertain this, we adopted a method which differs slightly from that applied by Tonry & Davis (1979; TD79 hereafter), but which proved to be quite effective to evidentitate discrepant templates. The first step was to cross-correlate the HD templates one against each other, assuming as correct radial velocities from the literature values. In Fig. 4(a) we plot the result of the cross-correlation, showing for each HD spectrum i the value of the quantity

$$\Delta v_{ij} = v_{ij} - v_i^{\rm lit},$$

i.e. the difference of the velocity of i measured by j and its literature value. Each mark in the plot is characterized by the value of j indicating the template which produced that value for the spectrum i reported on the abscissa. The underlying hypothesis is that if only random errors are present, the Δv_{ij} should be nearly normally distributed around zero, with a dispersion of the order of that expected from the resolution of the HD spectra, $\sigma \sim 25$ km s^{-1}. It is clear from the figure that this is not the case for some of the objects analysed. Qualitatively, the barycentre of the distributions of the Δv_{ij} is significantly different from zero for about half of the spectra, and the distributions are not fully symmetric. The global indication of the figure is that some of the HD spectra do have some significant shift with respect to their literature redshift. In particular, it is clear the tendency of #8 to overestimate the redshifts of the other spectra, while the measurements using #1 are systematically underestimated. Given the small number statistics and the possible asymmetry of the distributions, it is clear that the mean value of the Δv_{ij} for each i cannot be considered as a robust estimator for the true zero-point velocity. A more sensible choice seems to be the median, which is not affected by the asymmetric tails produced by the presence of a small number (1–2 in our case) of very discrepant templates (like, e.g., #8). We therefore determined a new value of $v_i^{\rm lit}$, by taking the median of the seven Δv_{ij} for each j. With these new values for each spectrum, we can construct new distributions of the Δv_{ij}, redetermine the median, and obtain new $v_i^{\rm lit}$. The procedure can be repeated a number of times, but essentially converges after only three iterations. In Fig. 4(b) we show the same plot of Fig. 4(a), after the third iteration. Note how the global scatter has been significantly reduced with respect to the first iteration, and is now compatible with that expected from the intrinsic resolution of the spectra. Essentially, the zero-point changed significantly only for three templates, as can be seen from Table 2. For the remaining spectra, the difference is less than 15 km s^{-1}, i.e. within the expected intrinsic uncertainty. These five spectra represent therefore a carefully tested set of templates with known radial velocity.

The idea is now to use these higher precision, well-calibrated templates to calibrate in turn the zero-point of the internal templates previously prepared. To this end, we ran the cross-correlation over the internal templates, using the five best HD as templates. For each internal spectrum, the velocity obtained with the best R value was chosen as zero-point (i.e. its 'literature' redshift), after checking the global consistency of the values obtained by the five templates. It is reassuring that the agreement among the five templates was very good, with typical rms discrepancies of around 10–15

Table 2. Characteristics – extracted from the Astronomical Almanac – of the high-quality external stellar templates. $v_{\rm lit}$ is the radial velocity as given in the Almanac, while $v_{\rm est}$ is the best value estimated here for the spectra at our disposal, following the minimization procedure described in the text.

Templ.	HD	α	δ	m_V	Type	v_{lit}	v_{est}
hd01	hd136202	15:18:49.7	01:48:03	5.06	F8IV–V	54	12
hd02	hd157457	17:25:15.5	−50:37:32	5.23	G8III	17	15
hd03	hd171391	18:34:30.7	−10:59:07	5.14	G8III	7	7
hd04	hd203638	21:23:37.4	−20:53:34	5.77	K0III	22	12
hd05	hd22484	03:36:23.2	00:22:19	4.28	F8V	28	15
hd06	hd26162	04:08:36.7	19:35:05	5.50	K1III	24	74
hd07	hd35410	05:23:59.9	−00:54:00	5.08	K0III	21	37
hd08	hd44131	06:19:31.0	−02:56:23	4.90	gM1	47	117

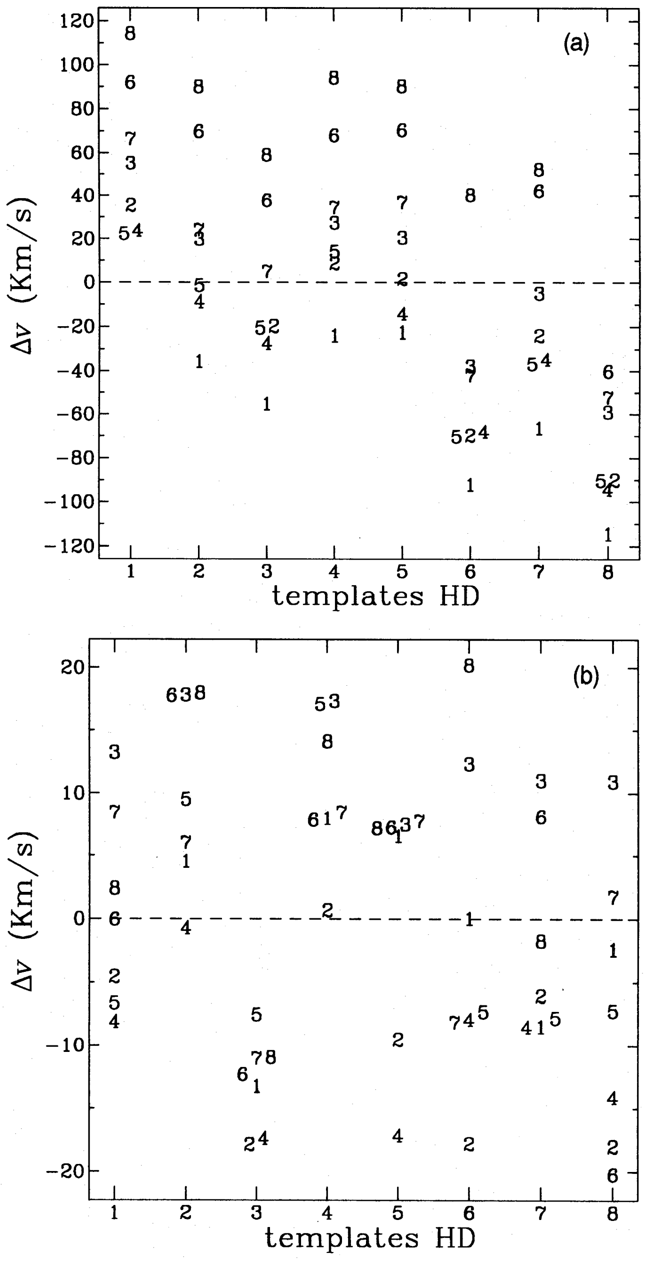

Figure 4. (a and b) Results of the cross-correlation among the high-quality HD spectra, showing for each spectrum i the value of the difference in the velocity of i as measured by j and its literature value. Each mark in the plot corresponds to the value of j indicating the template which produced that value for the spectrum i reported on the abscisssa (see text for details).

Table 3. The final set of 17 templates adopted for our measures, together with the two best-performing HD templates, hd02 and hd07. v_o is the proper radial velocity of each template, calibrated as described in the text. σ_v is the variance among the values of v_o given by the five different HD zero-point calibrators. The small values of σ_v are an indication of the precision attained in the overall procedure.

Name	v_o	σ_v
t00	7	14
t03+	21	12
t51	-8	14
t91	-6	15
t000+	35	15
t209+	45	11
t231+	54	8
t391+	5	12
t452+	24	14
PL11–11	18908	4
PL11–21	10189	15
PW5–14	28416	5
PL2–20	37198	19
PL2–27	8237	7
N5921	1500	11
N6070	2004	20
N6118	1533	26

km s^{-1}. Table 3 reports the final radial velocities for the set of internal templates, together with the rms value of the differences between the five measurements and their mean. In the same table we list also the three high S/N galaxies from Collins et al. (1995), which were included among the used templates to provide three external reference galaxies. These proved to be useful – despite a slightly lower intrinsic resolution – for corroborating the significance of uncertain redshifts for which the unanimity of the internal templates could be seen as suspect. In addition, we included in the final set of templates used for the cross-correlation with the survey spectra the two best performing HD stars, HD02 and HD07, for a total of 19 spectra.

3.4 Redshift measurement

As we have seen, the redshifts were measured using the cross-correlation technique discussed in detail by TD79, in the version developed at the Smithsonian Astrophysical Observatory as a subpackage of IRAF – called RVSAO – which closely follows the original prescription. Briefly, the cross-correlation of the observed galaxy spectrum with the template spectrum is accomplished by taking the fast Fourier transform (FFT) of the two spectra, multiplying the two FFTs, and then transforming back the result to get the cross-correlation function (CCF). The highest peak of the CCF is related to the radial velocity difference between the two spectra. Before actually starting this machinery, the two spectra are rebinned into logarithmic bins, so that the relative redshift becomes a linear shift between the two, and a number of operations are performed on them to improve the quality of the final result. These are described in detail by TD79, and include continuum subtraction, cosine-bell apodizing and bandpass filtering. RVSAO provides a user-friendly interface and the possibility to check all the intermediate steps, as well as to try several experiments to find the best set of parameters. Specifically, the spectra were rebinned into 4096 logarithmic bins, which corresponded to a formal velocity binwidth of ~35 km s^{-1}. The spectra were then filtered in order to eliminate both the low-frequency spurious components left by the subtracted continuum and the high-frequency binning noise. The best set of filter parameters was chosen to maximize the significance of the CCF. The peak of the CCF is fit by a quadratic polynomial, determining both the wavelength shift (from its position) and an estimate of the error ε (from its width). In its output, together with the value of cz, the program provides the value of ε, of the peak height, and of the confidence parameter R, that, as defined by TD79, corresponds to the ratio between the height of the highest peak in the CCF and the average value of the adjacent background.

After a first test run, the cross-correlation routine was run over the whole set of available spectra, including about 1000 spectra. The results obtained were scrutinized one by one, and ambiguous cases were re-examined directly. Spectra with $R<3$ were typically discarded. The result was considered significant only when at least half of the templates indicated a similar velocity, with the further constraint that these should not be templates of the same origin (e.g. all internal stars). We found, indeed, a tendency for 'similar' templates to be sometimes biased towards similar values, certainly because of some specific instrumental features not removed during the continuum subtraction and filtering phases. This is particularly true when $R\sim 3$, i.e. for very low S/N spectra. In general, measurements with $R<4$, although included in the final list, have to be regarded with some suspicion considering their low level of significance (see also Fig. 3).

Some objects were observed twice. The two estimates, if in agreement within the error limits, were averaged each with its own weight. If they were in disagreement, then that with the highest confidence parameter was chosen.

4 THE DATA

The final galaxy data are presented in Tables 4(a)–(d), subdivided among the four different regions. The columns are

Table 4. (a) Redshifts for the galaxies observed in the PW region. Radial velocities and the corresponding 1σ errors are in km s^{-1}.

RA	DEC	bj	vel	err	R
22:35:11.8	-28:00:41	–	20316	62	6.44
22:35:34.7	-28:13:12	–	105	34	7.26
22:35:41.0	-28:09:51	18.4	26597	56	4.67
22:35:43.2	-28:01:05	18.0	41915	120	3.12
22:35:53.7	-27:59:44	19.2	3097	114	3.17
22:35:55.0	-27:51:20	18.7	12326	123	6.26
22:35:55.9	-27:48:39	18.8	39845	69	5.25
22:36:00.6	-27:50:58	19.1	30792	73	6.90
22:36:00.7	-28:11:29	–	28163	59	3.66
22:36:02.4	-28:26:18	17.5	25544	45	7.80
22:36:12.1	-28:22:36	18.3	37144	54	4.02
22:36:13.4	-28:08:19	19.1	28945	68	6.51
22:36:17.0	-28:13:08	18.9	28526	70	2.94
22:36:18.3	-28:07:19	18.8	30083	184	3.62
22:36:19.2	-27:57:36	18.6	40070	44	5.61
22:36:21.2	-27:56:12	18.7	30798	94	5.75
22:36:28.7	-28:24:34	17.8	21389	35	8.22

Table 4 (a) – *continued*

RA	DEC	bj	vel	err	R
22:36:31.4	-28:11:14	19.2	8562	53	4.54
22:36:35.4	-28:00:33	18.3	30571	36	12.07
22:36:38.6	-28:14:37	16.9	14793	35	15.89
22:36:41.9	-27:52:25	18.6	15552	127	2.97
22:36:57.2	-28:03:53	18.6	28416	27	9.58
22:37:10.0	-28:45:41	–	39380	76	3.29
22:37:20.7	-28:27:53	19.3	30708	90	5.63
22:37:25.6	-28:19:42	17.5	23437	36	8.38
22:37:28.6	-28:27:53	17.8	3704	108	3.06
22:37:30.4	-27:55:29	17.4	41558	79	3.10
22:37:33.5	-28:01:55	18.2	29664	82	3.24
22:37:33.6	-28:26:48	18.8	14872	128	3.17
22:37:36.0	-28:16:10	17.2	14762	46	11.42
22:37:42.2	-28:25:47	18.7	40996	36	9.84
22:37:42.7	-28:56:30	16.9	78410	45	3.72
22:37:46.1	-28:03:00	18.5	29056	56	8.05
22:37:48.6	-28:38:07	18.3	35863	100	2.87
22:37:58.4	-28:11:29	–	44390	157	3.77
22:37:58.4	-27:49:53	–	24054	51	5.64
22:37:59.7	-28:34:01	18.5	27449	68	5.12
22:38:01.1	-28:21:24	19.1	57073	54	4.26
22:38:04.6	-27:57:24	18.4	23924	63	3.99
22:38:05.8	-28:34:09	18.5	12324	222	4.21
22:38:08.7	-28:39:17	19.00	35777	98	2.46
22:38:10.5	-28:35:10	19.2	28388	83	2.94
22:38:11.7	-27:51:32	16.5	17609	111	2.51
22:38:12.4	-27:54:52	18.8	56912	66	6.66
22:38:16.0	-28:08:17	18.3	2829	160	3.14
22:38:21.1	-28:22:01	19.0	24395	68	3.40
22:38:24.0	-28:11:03	17.3	11801	112	4.94
22:38:27.7	-28:01:42	18.6	40435	152	4.18
22:38:28.2	-27:50:32	18.8	69167	87	3.10
22:38:30.1	-28:55:26	19.1	29111	73	5.65
22:38:34.9	-28:23:46	19.2	40531	34	8.50
22:38:35.3	-28:13:48	17.7	17893	107	3.55
22:38:41.0	-28:17:40	18.9	40685	106	2.95
22:38:46.9	-27:59:07	18.1	29871	74	5.62
22:38:57.8	-28:30:38	17.9	23278	111	3.15
22:38:57.9	-28:33:59	–	29701	117	3.18
22:39:04.4	-28:24:47	17.8	14988	111	4.47
22:39:06.2	-28:24:00	16.1	14907	37	11.00
22:39:30.1	-28:12:33	18.6	28666	29	13.45

Table 4. (b) Redshifts for the galaxies observed in the PL region. Radial velocities and the corresponding 1σ errors are in km s^{-1}.

RA	DEC	bj	vel	err	R
23:39:06.4	-28:53:29	19.2	30540	71	5.84
23:39:07.6	-28:41:28	19.1	64782	234	2.39
23:39:08.2	-28:08:05	19.6	64936	136	2.23
23:39:15.4	-28:06:55	19.5	69791	125	4.31
23:39:22.2	-27:50:26	19.4	72232	146	2.55
23:39:25.2	-28:58:29	19.0	46686	107	4.24
23:39:30.5	-27:56:52	19.3	30406	79	5.42
23:39:36.0	-28:10:11	17.0	8341	39	10.90

Table 4 (b) – *continued*

RA	DEC	bj	vel	err	R
23:39:42.3	-28:51:57	19.5	30618	96	3.17
23:39:42.8	-28:12:54	18.0	25653	198	3.18
23:39:46.1	-28:52:48	19.3	37086	71	5.01
23:39:49.9	-27:56:53	19.6	70242	69	3.49
23:39:53.0	-28:11:17	17.7	34433	59	9.60
23:39:53.2	-28:51:32	19.2	30812	107	2.75
23:39:57.1	-28:22:50	18.4	50595	172	3.04
23:39:58.3	-28:26:51	18.7	51143	94	2.56
23:39:58.4	-28:25:58	19.3	68988	75	3.61
23:39:59.3	-28:08:44	17.5	15332	41	10.45
23:40:00.2	-28:18:27	19.0	25996	149	2.80
23:40:01.3	-28:30:28	17.7	25175	191	3.82
23:40:06.8	-28:09:07	16.9	8829	55	4.20
23:40:07.7	-28:58:23	19.4	30643	82	3.59
23:40:09.4	-28:56:15	19.5	30649	75	2.87
23:40:09.7	-28:29:09	19.3	54894	67	6.19
23:40:12.2	-28:45:58	19.3	63483	69	5.96
23:40:14.0	-28:44:52	18.0	8558	57	3.67
23:40:14.8	-28:43:45	18.5	35395	78	8.26
23:40:20.0	-27:54:58	18.3	41527	81	2.74
23:40:25.8	-28:16:43	18.1	8586	48	3.17
23:40:27.2	-28:54:03	19.2	30895	120	3.05
23:40:27.6	-27:58:43	18.3	19310	49	10.50
23:40:31.6	-28:38:18	19.4	30656	80	4.40
23:40:32.1	-28:54:14	19.4	30727	106	3.23
23:40:32.3	-27:53:53	18.3	20204	65	7.25
23:40:33.8	-27:58:45	18.9	32142	106	3.03
23:40:34.0	-28:13:57	18.9	56929	333	3.86
23:40:35.4	-28:18:20	17.5	8293	67	7.28
23:40:35.6	-28:19:27	19.5	16136	57	4.03
23:40:38.1	-28:38:02	18.3	30514	84	5.49
23:40:38.3	-28:25:23	18.8	36238	53	6.22
23:40:38.4	-27:53:03	19.3	19790	82	3.14
23:40:38.9	-28:31:05	17.6	8296	42	5.38
23:40:41.3	-28:38:25	17.5	15912	81	4.35
23:40:44.1	-28:49:38	19.6	42085	132	3.28
23:40:44.3	-28:29:16	19.4	29127	61	8.11
23:40:45.2	-27:56:45	18.3	25191	51	8.20
23:40:45.3	-28:19:57	18.0	19059	99	2.65
23:40:46.7	-28:27:56	18.0	8451	96	4.99
23:40:51.7	-28:35:15	19.4	44801	47	4.85
23:40:55.7	-28:12:23	–	53414	79	3.38
23:40:58.4	-28:16:23	19.1	34362	42	10.38
23:40:59.2	-28:22:42	17.0	8574	98	3.58
23:41:02.5	-28:31:44	18.8	53146	64	3.70
23:41:03.0	-27:56:24	19.1	53463	124	3.06
23:41:05.0	-28:28:29	16.4	15902	43	9.63
23:41:08.7	-28:27:45	19.0	24150	88	3.13
23:41:10.1	-28:23:08	18.7	15950	133	3.03
23:41:14.2	-28:43:11	19.1	30482	47	8.53
23:41:14.3	-28:43:42	19.3	20430	37	8.01
23:41:14.9	-28:45:10	19.4	13111	147	3.78
23:41:19.1	-28:39:52	18.2	37198	32	8.40
23:41:19.3	-28:31:52	19.1	35308	137	2.47
23:41:19.4	-28:22:29	17.2	8620	84	4.61
23:41:20.2	-28:55:39	19.0	3460	80	2.85

Table 4 (b) – *continued*

RA	DEC	bj	vel	err	R
23:41:20.9	-28:33:11	19.2	63247	125	3.76
23:41:24.5	-28:24:10	18.9	44845	73	5.34
23:41:29.6	-28:08:01	18.8	65301	44	3.76
23:41:34.1	-28:34:35	15.9	8237	19	19.27
23:41:34.4	-28:48:23	19.5	45652	102	2.89
23:41:40.7	-27:48:20	19.2	55990	141	4.27
23:41:41.6	-27:55:55	17.7	16032	36	13.19
23:41:42.6	-28:36:42	18.9	30557	58	7.92
23:41:43.9	-28:46:08	19.3	54748	53	6.18
23:41:45.9	-28:28:24	17.9	8398	67	3.84
23:41:46.1	-27:48:18	19.5	63991	80	7.50
23:41:46.3	-27:56:13	17.2	16145	166	3.18
23:41:49.7	-28:03:49	19.6	64439	46	4.92
23:41:53.6	-28:24:47	16.4	8377	90	4.90
23:41:54.7	-28:07:00	16.8	22506	51	9.70
23:41:57.3	-28:41:11	19.2	45714	83	2.88
23:41:59.3	-28:11:51	19.6	63010	145	3.48
23:42:01.9	-28:03:13	19.3	66106	89	2.57
23:42:02.6	-27:56:13	16.3	9063	34	12.65
23:42:05.1	-28:15:54	17.2	15985	27	10.45
23:42:06.5	-28:43:30	18.9	35399	61	5.86
23:42:08.4	-28:40:04	17.8	35336	44	4.49
23:42:12.4	-28:19:23	18.4	23764	79	3.92
23:42:12.9	-28:27:00	19.5	17915	82	2.97
23:42:15.1	-28:12:48	19.2	55305	79	3.37
23:42:15.8	-28:57:47	19.4	45018	123	3.94
23:42:17.4	-28:30:44	18.5	18949	55	11.00
23:42:19.9	-28:20:32	18.9	17667	92	2.62
23:42:26.3	-28:40:42	19.0	45088	103	2.88
23:42:27.5	-28:15:51	18.2	8742	96	4.51
23:42:31.1	-28:20:09	17.7	19134	37	10.88
23:42:32.4	-28:32:52	16.6	8230	17	26.71
23:42:40.2	-28:28:55	19.4	30327	85	5.06
23:42:43.6	-28:21:02	18.2	37627	89	4.62
23:42:43.6	-27:52:21	19.1	22353	80	5.30
23:42:46.9	-28:02:33	19.4	10347	76	2.98
23:42:50.6	-28:05:00	17.7	31219	118	3.56
23:42:51.8	-28:14:28	16.9	8933	35	14.10
23:42:53.8	-28:33:59	–	34869	117	3.28
23:42:54.9	-28:48:15	19.6	37152	42	4.81
23:42:58.3	-28:14:21	18.8	32743	35	9.47
23:42:58.3	-28:27:27	17.9	8404	30	9.54
23:42:59.5	-28:14:00	18.4	32241	118	4.44
23:43:02.0	-28:31:11	18.3	30528	68	7.98
23:43:03.1	-28:00:41	–	88529	127	3.49
23:43:04.1	-28:23:45	19.4	84917	123	1.87
23:43:05.0	-28:05:07	17.9	9115	76	6.85
23:43:06.0	-28:48:57	18.4	12094	176	2.80
23:43:11.8	-28:08:36	19.3	33643	78	3.09
23:43:12.7	-28:33:33	19.3	28803	61	6.37
23:43:15.2	-28:35:50	19.5	20009	227	3.80
23:43:16.4	-28:19:32	18.0	8917	52	4.28
23:43:17.2	-27:51:46	17.8	35403	61	5.86
23:43:17.6	-28:35:14	18.3	64808	113	2.91
23:43:18.3	-28:19:04	19.1	44402	97	3.99
23:43:18.4	-28:29:21	18.9	15688	115	2.69

Table 4 (b) – *continued*

RA	DEC	bj	vel	err	R
23:43:19.0	-28:41:46	18.5	29022	69	3.36
23:43:19.3	-28:55:35	19.2	68137	65	3.13
23:43:19.5	-27:59:51	18.0	7760	85	5.05
23:43:19.6	-28:30:31	18.8	7572	200	3.56
23:43:19.8	-28:52:40	17.0	15649	48	6.53
23:43:20.0	-28:05:59	19.2	70159	87	6.72
23:43:23.8	-28:06:24	18.0	35437	56	8.65
23:43:24.7	-28:10:23	17.6	8615	24	18.45
23:43:25.7	-28:50:49	19.5	68228	80	2.74
23:43:26.3	-28:28:07	19.4	79760	67	3.08
23:43:26.5	-27:50:25	19.6	42075	147	3.10
23:43:26.7	-28:31:46	19.5	55561	106	3.77
23:43:27.0	-28:06:16	19.2	35605	85	5.92
23:43:33.0	-28:22:10	18.7	35484	101	3.21
23:43:33.4	-28:19:50	18.9	35330	51	6.43
23:43:35.4	-28:35:24	19.0	55436	94	4.40
23:43:36.4	-28:22:49	18.7	35048	60	6.23
23:43:36.8	-27:55:01	19.4	53693	164	2.84
23:43:37.0	-28:19:14	19.0	34947	81	6.29
23:43:37.3	-28:36:17	18.9	61873	190	2.44
23:43:37.8	-27:55:56	19.0	53854	58	4.41
23:43:39.8	-28:23:16	18.5	3909	93	2.75
23:43:39.9	-28:19:38	18.2	35422	60	8.15
23:43:40.6	-27:53:31	18.6	92202	182	2.30
23:43:40.8	-27:54:46	18.0	28661	102	3.33
23:43:41.2	-28:07:52	18.4	41557	91	3.13
23:43:42.3	-28:18:45	18.5	35344	50	5.30
23:43:42.9	-28:23:11	–	43698	57	3.73
23:43:44.7	-28:36:55	18.6	19206	73	6.21
23:43:45.6	-28:38:53	19.3	23902	74	2.85
23:43:45.7	-28:36:10	19.5	53555	76	4.42
23:43:48.9	-27:58:20	19.4	48027	127	2.55
23:43:50.0	-28:23:19	19.3	86965	86	2.93
23:43:51.6	-28:25:45	19.6	32413	69	4.22
23:43:52.0	-28:49:58	18.9	20921	47	5.79
23:43:52.0	-27:49:53	18.4	41557	91	3.13
23:43:52.3	-28:24:17	19.5	35142	72	4.59
23:43:53.1	-28:52:12	19.1	20768	60	3.36
23:43:53.7	-28:56:29	–	62095	78	3.66
23:43:54.1	-28:32:47	18.4	6829	99	2.91
23:43:57.0	-28:30:56	18.8	63500	85	4.52
23:44:01.4	-28:23:05	19.3	65324	67	3.47
23:44:03.5	-28:56:33	19.1	38758	96	5.37
23:44:04.1	-28:28:29	18.3	43467	100	5.00
23:44:04.9	-28:19:44	19.3	43539	41	7.31
23:44:07.4	-28:12:41	18.5	9328	81	6.01
23:44:09.4	-28:52:24	18.9	87983	46	3.90
23:44:09.8	-28:06:03	18.8	20855	84	3.88
23:44:10.8	-28:40:25	19.1	62886	80	6.45
23:44:14.6	-28:51:50	18.0	5799	81	3.08
23:44:17.1	-27:51:27	17.0	9404	85	4.44
23:44:18.2	-27:58:36	18.2	31048	90	5.39
23:44:19.7	-28:35:05	19.5	65906	177	3.31
23:44:25.6	-28:38:44	18.5	92924	87	3.47
23:44:25.7	-28:22:32	19.6	47829	56	10.15
23:44:27.1	-28:14:08	18.7	20880	67	5.13

Table 4 (b) – *continued*

RA	DEC	bj	vel	err	R
23:44:27.6	-28:33:45	19.6	55089	102	4.11
23:44:28.8	-28:19:39	18.8	28651	89	3.08
23:44:32.5	-28:38:04	19.5	65938	119	1.93
23:44:36.1	-28:16:22	19.2	15173	96	3.08
23:44:37.1	-28:00:41	19.2	42382	138	3.30
23:44:37.4	-28:29:27	18.4	18889	41	10.99
23:44:40.7	-28:34:07	19.6	66252	77	3.16
23:44:44.2	-28:26:32	19.6	65957	105	5.81
23:44:45.3	-28:24:19	19.2	63420	62	3.82
23:44:45.6	-28:46:35	18.7	16063	133	2.90
23:44:46.0	-28:19:54	19.0	9634	87	4.50
23:44:51.3	-28:30:35	19.3	35258	73	5.81
23:44:51.9	-28:12:23	–	35822	75	3.45
23:44:54.3	-27:56:23	15.9	8560	39	11.02
23:44:54.9	-28:12:45	18.8	8209	95	3.11
23:44:56.3	-28:46:23	19.5	66604	61	3.73
23:44:57.1	-28:26:06	19.3	54592	88	4.60
23:45:04.0	-28:22:51	18.3	58037	132	2.29
23:45:04.0	-28:04:05	19.2	9415	63	2.64
23:45:06.2	-28:45:38	17.9	15292	111	4.22
23:45:06.5	-28:29:15	19.0	30138	42	11.46
23:45:08.1	-28:12:43	19.5	12104	266	3.73
23:45:09.7	-28:06:29	18.2	9610	47	5.20
23:45:18.0	-28:47:41	19.5	62689	92	6.20
23:45:18.7	-28:19:00	19.4	88537	62	3.57
23:45:18.8	-27:58:22	16.9	15135	77	4.28
23:45:20.0	-28:31:05	18.9	9550	85	4.79
23:45:20.3	-28:13:54	17.2	10656	44	10.78
23:45:20.7	-28:48:39	19.2	68932	77	5.95
23:45:20.8	-28:44:24	19.4	65486	173	4.04
23:45:25.6	-28:50:31	17.9	8630	48	9.79
23:45:25.7	-28:18:54	19.3	43617	63	5.99
23:45:25.9	-28:11:59	17.8	15016	54	8.23
23:45:28.5	-28:25:57	19.2	35293	51	10.93
23:45:33.1	-28:01:20	18.0	27833	96	3.03
23:45:33.9	-28:40:01	19.1	20048	101	3.51
23:45:38.1	-28:24:03	18.8	8891	43	10.64
23:45:38.4	-28:48:07	18.1	9530	138	2.70
23:45:43.8	-28:08:04	18.3	28607	137	3.09
23:45:44.5	-28:11:51	18.5	10330	66	7.65
23:45:48.7	-28:43:48	19.3	81356	88	4.47
23:45:51.4	-28:04:24	19.5	3209	105	2.37
23:45:52.3	-28:30:41	19.0	19708	75	2.87
23:45:54.0	-28:41:53	18.9	67182	51	4.06
23:45:55.7	-28:39:38	18.8	24330	112	3.50
23:46:01.8	-28:40:30	19.2	19526	195	2.44
23:46:12.4	-27:52:37	16.7	19300	34	13.47
23:46:13.1	-27:58:38	18.3	28522	159	3.09
23:46:14.5	-27:49:24	18.0	33447	72	7.01
23:46:14.7	-28:55:41	16.5	10594	49	7.74
23:46:19.5	-27:54:12	16.8	19508	50	7.24
23:46:21.0	-28:51:38	19.3	74715	109	2.32
23:46:22.1	-28:40:13	19.0	75092	143	2.34
23:46:22.7	-28:56:47	19.5	44817	131	2.71
23:46:24.1	-28:52:15	16.8	19092	31	13.90
23:46:26.3	-28:41:00	18.3	9464	136	4.35

Table 4 (b) – *continued*

RA	DEC	bj	vel	err	R
23:46:27.7	-28:52:23	18.0	16994	107	4.02
23:46:29.5	-28:01:27	19.3	65047	92	2.43
23:46:35.6	-27:55:46	18.3	8681	56	7.08
23:46:37.1	-28:53:36	19.4	20598	97	3.29
23:46:39.9	-28:15:14	16.1	10253	45	10.94
23:46:44.0	-28:49:45	18.8	20743	86	4.13
23:46:45.8	-28:49:10	17.0	8678	67	5.81
23:47:00.7	-28:31:05	17.9	9522	62	7.61
23:47:07.5	-28:27:49	18.1	8525	96	2.85
23:47:08.9	-28:19:44	17.0	9187	51	8.25
23:47:09.2	-28:32:22	17.9	8560	107	3.34
23:47:09.2	-28:17:00	18.7	10067	70	3.41
23:47:10.5	-27:58:45	16.7	19197	133	3.53
23:47:11.1	-28:51:49	19.3	28341	47	4.50
23:47:12.4	-28:32:53	18.7	21888	89	3.74
23:47:13.6	-28:11:15	17.0	19400	87	2.41
23:47:13.9	-28:25:20	19.1	25194	114	2.75
23:47:15.7	-28:13:44	15.4	8855	34	13.72
23:47:19.2	-28:23:12	18.1	97333	157	3.60
23:47:19.8	-27:54:49	18.8	32554	146	2.72
23:47:20.5	-28:09:07	17.0	17717	119	3.75
23:47:22.2	-28:23:51	19.1	28517	63	4.79
23:47:24.7	-28:28:06	17.4	15860	135	2.91
23:47:25.0	-28:08:39	19.2	82046	147	3.09
23:47:30.6	-28:31:30	19.0	33025	90	2.66
23:47:33.0	-28:49:23	19.4	20509	65	3.20
23:47:33.4	-28:22:06	19.2	41874	107	2.44
23:47:37.1	-28:17:13	18.6	28824	49	5.08
23:47:40.1	-28:42:46	18.8	51379	79	4.40
23:47:41.7	-28:54:32	18.5	26200	115	3.41
23:47:42.1	-28:05:50	17.3	35849	83	3.14
23:47:42.5	-28:35:25	18.7	3270	88	2.93
23:47:45.6	-28:45:58	19.4	19897	78	3.14
23:47:46.1	-28:37:16	18.8	97605	50	3.46
23:47:47.5	-27:49:53	–	39633	68	3.16
23:47:49.3	-28:13:06	15.9	8659	76	4.46
23:47:50.5	-28:42:36	17.3	28484	77	4.77
23:47:54.6	-28:42:20	17.1	8253	62	7.81
23:47:55.7	-27:58:47	17.7	18120	180	3.30
23:47:56.0	-28:39:39	17.6	19217	59	4.64
23:47:58.7	-28:54:43	18.5	76635	99	2.73
23:47:59.9	-28:04:19	16.4	8880	57	9.53
23:48:00.3	-28:42:39	17.9	11388	67	3.86
23:48:01.8	-28:52:35	18.5	8490	88	5.23
23:48:02.7	-28:42:46	15.5	8457	61	6.52
23:48:05.1	-28:24:47	19.4	29043	154	3.98
23:48:06.4	-28:36:44	18.8	19042	101	3.79
23:48:17.5	-27:55:15	18.1	21922	108	4.19
23:48:17.6	-28:20:10	17.7	8290	53	7.61
23:48:18.8	-28:26:36	17.0	17567	83	3.69
23:48:20.4	-28:45:39	17.8	19106	44	9.46
23:48:21.2	-28:07:05	18.8	45841	129	3.19
23:48:21.9	-28:34:39	18.8	64341	248	3.52
23:48:22.2	-28:51:49	18.8	76747	78	3.22
23:48:22.8	-28:16:13	17.8	30371	138	4.35
23:48:25.2	-28:13:01	16.5	9011	39	9.80

Table 4 (b) – *continued*

RA	DEC	bj	vel	err	R
23:48:28.3	-28:37:41	16.7	8379	79	4.31
23:48:31.0	-28:36:22	19.6	11368	88	3.77
23:48:31.7	-28:50:00	19.1	8307	48	10.36
23:48:32.7	-28:34:23	17.3	18984	59	9.38
23:48:35.9	-28:45:27	19.6	11378	74	3.59
23:48:36.2	-28:35:21	17.6	18908	25	15.79
23:48:39.3	-28:37:11	17.2	11351	99	2.73
23:48:40.6	-28:11:26	19.5	65226	113	3.05
23:48:41.9	-28:35:12	19.0	21713	51	10.06
23:48:43.8	-28:15:09	16.1	10189	28	19.74
23:48:44.7	-28:41:51	19.2	4717	73	3.32
23:48:45.8	-28:48:29	16.2	8439	108	3.49
23:48:48.2	-28:12:23	–	23608	80	3.62
23:48:50.3	-28:45:32	17.8	57994	93	3.20
23:48:51.6	-28:19:48	17.7	9687	45	9.00
23:48:55.0	-28:32:04	19.0	64164	80	3.78
23:48:58.5	-28:17:34	19.3	47245	120	3.81
23:48:59.3	-28:20:59	16.0	9711	40	13.44
23:48:59.9	-28:48:32	19.6	20986	80	3.42
23:48:60.0	-28:21:26	16.5	8591	38	12.49
23:49:00.3	-28:33:54	17.8	8544	40	13.12
23:49:01.5	-28:38:35	14.2	8285	30	18.14
23:49:02.2	-28:19:47	17.9	10149	64	6.46
23:49:03.3	-28:17:31	17.8	9146	86	3.11
23:49:06.6	-28:21:07	19.1	10011	63	7.40
23:49:15.0	-28:34:18	17.6	8360	55	4.49
23:49:15.1	-28:14:36	15.8	8862	38	11.30
23:49:15.7	-27:52:31	17.1	65270	67	2.86
23:49:17.5	-28:31:55	18.0	7629	231	2.73
23:49:19.0	-28:35:37	19.2	82073	102	2.30
23:49:19.2	-28:12:29	15.3	8866	36	14.44
23:49:19.3	-28:15:44	18.6	20533	66	2.88
23:49:26.8	-28:28:15	17.7	9372	47	9.86
23:49:27.0	-28:47:35	19.0	17153	54	5.23
23:49:31.8	-28:45:16	18.1	8683	70	3.83
23:49:33.3	-28:51:50	19.3	32700	118	3.58
23:49:38.9	-28:57:37	19.3	25343	120	2.81
23:49:43.7	-28:46:42	19.5	52310	205	2.88
23:49:44.0	-28:34:12	17.1	9592	90	4.27
23:49:48.7	-28:37:16	18.7	67683	66	3.21
23:49:49.4	-28:33:31	17.9	18499	223	2.78
23:49:50.7	-27:54:27	19.6	73122	64	3.11
23:49:51.1	-27:55:01	16.4	8880	62	7.92
23:49:52.5	-28:53:08	17.6	17550	68	4.71
23:49:53.2	-28:40:49	18.7	17997	40	6.58
23:49:53.4	-28:53:13	18.3	18614	43	10.42
23:49:54.7	-28:56:11	19.3	21029	64	3.77
23:49:54.9	-28:37:15	15.8	8516	42	8.66
23:49:56.3	-28:15:54	17.5	19309	143	2.59
23:49:58.2	-28:57:43	18.1	18024	56	5.44
23:50:02.3	-28:54:46	19.4	63505	90	3.01
23:50:02.7	-28:16:01	19.6	94794	92	2.18
23:50:03.1	-28:49:20	17.2	18520	101	4.00
23:50:03.3	-28:14:04	18.4	21868	109	3.92
23:50:05.6	-28:15:35	18.0	21626	38	11.17
23:50:08.4	-28:46:16	16.6	17586	54	11.16

Table 4 (b) – *continued*

RA	DEC	bj	vel	err	R
23:50:09.1	-28:50:55	15.6	17522	59	10.02
23:50:10.1	-28:54:21	19.1	18536	119	4.53
23:50:10.4	-27:49:06	19.4	35621	82	2.79
23:50:10.5	-28:52:14	18.1	17898	116	3.57
23:50:11.3	-28:57:39	19.0	80708	63	2.87
23:50:13.4	-27:49:14	18.8	11691	161	3.97
23:50:16.1	-28:12:48	17.2	19713	120	3.31
23:50:17.6	-28:26:20	19.5	68203	86	3.10
23:50:22.9	-28:37:34	19.6	29338	79	4.14
23:50:23.8	-28:48:09	18.7	4765	73	3.98
23:50:25.0	-28:42:17	17.3	19238	49	11.79
23:50:34.1	-27:57:00	18.7	59415	74	3.41
23:50:37.2	-28:26:12	19.2	28454	88	3.28
23:50:40.4	-28:32:06	17.2	22002	66	7.13
23:50:48.8	-28:01:26	18.6	97929	70	3.47
23:51:00.2	-28:28:01	19.1	56166	63	5.60
23:51:00.9	-28:18:59	18.7	46527	259	2.66
23:51:01.6	-28:31:47	17.1	94481	90	3.95

Table 4. (c) Redshifts for the galaxies observed in the FD region. Radial velocities and the corresponding 1σ errors are in km s^{-1}.

RA	DEC	bj	vel	err	R
2:02:04.6	-29:57:04	18.0	18625	86	6.18
2:02:13.1	-29:20:11	19.1	59568	74	3.07
2:02:20.7	-29:15:41	18.6	18981	77	3.94
2:02:23.2	-29:54:31	19.5	53976	105	4.03
2:02:24.5	-29:16:35	16.2	18860	112	3.30
2:02:25.0	-29:44:58	19.2	46725	109	2.60
2:02:38.4	-29:26:20	17.0	63148	67	3.03
2:02:45.5	-29:26:42	19.4	58939	77	3.30
2:02:52.9	-29:24:42	19.2	51570	119	4.20
2:02:55.9	-29:15:39	18.8	153522	29	18.25
2:02:56.4	-29:37:13	19.4	8995	79	2.58
2:02:56.6	-30:04:36	–	16582	77	3.43
2:02:56.6	-29:43:00	–	41509	141	2.97
2:02:57.3	-29:57:14	18.2	25320	113	2.95
2:03:04.1	-29:23:48	18.7	24569	94	2.69
2:03:06.5	-29:35:32	18.7	44558	69	5.51
2:03:06.5	-29:32:49	19.2	68931	104	2.90
2:03:07.5	-29:34:13	17.7	17369	51	9.73
2:07:45.8	-29:01:19	18.8	91356	55	3.98
2:08:04.1	-29:06:26	18.8	77304	64	2.91
2:08:21.3	-29:09:54	18.3	32960	96	3.60
2:08:29.3	-29:09:17	18.6	7297	112	2.89
2:08:33.3	-29:02:07	19.4	27669	64	3.17
2:08:35.6	-28:55:56	19.4	50851	210	3.19
2:08:36.3	-28:58:31	18.0	40664	115	3.01
2:08:47.4	-29:28:37	18.4	88608	109	2.96
2:08:48.1	-29:33:46	19.0	44486	181	2.76
2:08:48.6	-28:44:49	19.5	37334	111	3.18
2:08:49.2	-29:13:59	19.4	21374	99	2.86
2:08:52.7	-28:48:20	–	27734	81	3.55
2:08:58.4	-29:13:22	18.8	70131	114	3.42
2:09:03.8	-28:52:22	17.9	27604	111	2.43

Table 4 (c) – *continued*

RA	DEC	bj	vel	err	R
2:09:03.8	-29:23:52	18.2	44158	116	3.34
2:09:06.2	-29:31:34	16.9	24741	68	7.22
2:09:06.4	-29:19:41	18.6	53926	126	2.49
2:09:11.3	-29:29:33	18.7	24914	71	3.14
2:09:11.4	-29:40:49	19.1	37881	121	3.30
2:09:14.9	-29:00:56	17.9	25195	109	3.09
2:09:21.1	-29:13:45	17.8	24386	64	3.29
2:09:23.1	-29:26:32	15.6	24495	91	5.68
2:09:36.6	-28:50:54	19.2	10904	86	2.42
2:09:48.4	-29:15:50	16.8	25084	117	2.45
2:10:20.6	-29:26:14	18.5	52878	108	2.96
2:10:28.7	-29:30:28	18.5	68309	68	3.42
2:14:35.3	-28:30:48	18.9	32469	94	3.90
2:14:51.7	-28:31:51	18.7	24730	89	3.22
2:14:58.9	-28:35:40	19.1	56186	37	6.04
2:15:01.8	-28:25:25	19.2	42936	95	3.09
2:15:06.1	-28:41:28	19.2	70554	109	3.25
2:15:06.5	-28:35:43	18.3	56733	146	4.38
2:15:08.8	-28:36:10	19.1	32034	124	4.20
2:15:16.5	-28:33:55	18.5	32462	104	5.76
2:15:35.5	-28:37:46	18.6	32452	65	6.00
2:15:37.2	-28:41:03	18.5	70499	70	3.00
2:15:50.0	-28:45:07	18.9	32275	47	5.75
2:16:02.0	-28:30:33	19.2	50521	61	4.35
2:16:05.7	-28:33:24	18.5	36383	58	6.37

Table 4. (d) Redshifts for the galaxies observed in the PE region. Radial velocities and the corresponding 1σ errors are in km s^{-1}.

RA	DEC	bj	vel	err	R
3:04:53.9	-28:45:28	19.2	68451	93	2.97
3:04:54.3	-28:52:51	19.0	78348	94	2.65
3:05:07.6	-28:57:34	19.1	56909	78	3.07
3:05:24.5	-28:51:32	19.4	40443	51	6.96
3:05:33.6	-28:39:27	18.4	46744	63	6.15
3:06:04.3	-28:52:53	18.2	21152	43	6.41
3:06:18.5	-28:46:05	19.5	47706	97	3.63
3:06:25.5	-28:43:54	19.0	43309	70	3.65
3:06:26.2	-28:48:42	18.6	20514	156	3.29

Table 4. (e) Redshifts for galaxies in the PL region from previous observations (see text).

RA	DEC	bj	vel	Notes
23:42:02.6	-27:56:13	16.3	9107	
23:43:06.8	-28:16:57	15.8	7551	
23:43:39.0	-28:22:35	15.4	8353	
23:43:59.7	-28:16:25	16.2	14827	
23:44:08.0	-28:36:47	–	7216	No EDSGC
23:44:35.4	-28:31:05	18.3	7457	
23:44:36.2	-28:12:28	16.3	8692	
23:44:36.4	-28:33:27	18.9	65170	
23:44:37.4	-28:17:42	17.0	10023	
23:44:38.4	-28:28:14	17.0	8724	

Table 4 (e) – *continued*

RA	DEC	bj	vel	Notes
23:44:38.8	-28:14:08	15.2	8424	
23:44:39.6	-28:36:55	19.2	53279	
23:44:40.5	-28:34:55	19.0	66321	
23:44:40.6	-28:34:13	18.9	66007	
23:44:40.9	-28:24:06	16.7	8826	
23:44:41.9	-28:37:06	19.0	64906	
23:44:44.2	-28:20:26	17.4	8092	
23:44:47.3	-28:23:48	16.5	9605	
23:44:48.0	-28:37:23	18.6	45242	
23:44:50.0	-28:00:00	–	8700	No EDSGC
23:44:52.0	-28:24:47	–	8012	No EDSGC
23:44:52.8	-28:24:48	15.1	8116	
23:44:53.0	-28:22:57	–	7805	Next to cD; No EDSGC
23:44:53.0	-28:22:59	–	10191	Next to cD; No EDSGC
23:44:53.2	-28:23:11	14.1	7990	cD galaxy
23:44:53.6	-28:28:40	18.4	18251	
23:44:54.0	-28:24:43	–	8065	No EDSGC
23:44:55.0	-28:24:01	–	8694	No EDSGC
23:44:55.0	-28:24:01	–	9582	No EDSGC
23:44:57.0	-28:23:12	–	8496	No EDSGC
23:44:57.1	-28:26:06	19.3	16295	
23:44:58.8	-28:25:55	17.9	9771	
23:44:59.6	-28:24:11	17.1	8301	
23:45:06.0	-28:24:18	–	8958	No EDSGC
23:45:07.2	-28:25:01	13.8	8554	IC5358 (VV13A)
23:45:07.4	-28:26:04	18.3	7826	
23:45:07.5	-28:27:02	16.6	8182	
23:45:08.9	-27:45:54	15.3	8505	
23:45:09.0	-28:26:30	–	9468	No EDSGC
23:45:09.2	-28:25:01	13.8	7972	VV13B; No EDSGC
23:45:09.9	-28:23:08	18.2	8021	
23:45:11.0	-28:24:47	–	8047	No EDSGC
23:45:12.0	-27:46:00	15.0	8866	
23:45:13.7	-28:21:52	17.6	9606	
23:45:14.5	-28:25:48	17.8	9998	
23:45:18.3	-28:26:36	17.5	9045	
23:45:20.2	-28:35:55	15.6	10095	
23:45:23.1	-28:25:11	16.6	7375	
23:45:29.3	-28:27:20	17.5	8216	
23:45:38.0	-28:41:34	17.1	15735	
23:45:43.3	-28:27:24	16.8	10320	
23:45:44.7	-28:30:36	15.5	8660	
23:45:45.3	-28:23:39	16.0	8923	
23:45:47.5	-28:21:10	15.5	10091	
23:45:50.0	-28:28:02	16.9	8830	
23:45:50.4	-28:33:23	16.6	8117	
23:45:50.7	-28:21:15	18.6	9614	
23:45:51.0	-28:25:49	–	9494	No EDSGC
23:46:16.0	-28:36:20	–	9411	No EDSGC
23:46:39.9	-28:15:14	16.1	10166	
23:47:15.7	-28:13:44	15.4	9028	
23:47:24.0	-28:13:00	15.0	8750	
23:47:49.3	-28:13:06	15.9	8718	
23:48:12.0	-28:43:00	15.00	16676	
23:48:43.8	-28:15:09	16.1	9947	
23:48:51.6	-28:19:48	17.7	10449	
23:48:56.0	-28:17:58	15.7	9501	
23:49:01.5	-28:38:35	14.2	7799	
23:49:15.1	-28:14:36	15.8	9038	
23:49:19.2	-28:12:29	15.3	8753	
23:49:24.0	-28:13:45	19.1	8899	
23:49:24.0	-28:12:00	–	8794	No EDSGC
23:49:41.1	-28:44:55	18.2	8814	
23:49:54.9	-28:37:15	15.8	7836	
23:51:52.8	-27:47:57	16.4	10215	
23:51:53.1	-27:47:59	–	14911	No EDSGC (blended)
23:51:53.2	-27:47:59	–	15106	No EDSGC
23:53:49.8	-28:46:25	16.4	9044	

Table 5. Estimation of the completeness in the four regions of the survey, at different magnitude cuts. The columns report: the number of fields per region (*no. fields*), the number of objects in the EDSGC photometric sample (n_{obj}^{EDSGC}), the number of misclassified stars (n_{stars}), the number of galaxy redshifts (n_z) out of the initial sample (stars are already excluded), the number of additional redshifts for objects which do not appear in the EDSGC ($n_z^{noEDSGC}$), and finally the completeness within the four regions. For PL (*) the magnitude limit in reality is 19.62 instead of 19.5 as for the other fields (see text for details).

region	no. fields	n_{obj}^{EDSGC}	n_{stars}	n_z	$n_z^{noEDSGC}$	compl (%)		
						≤ 19.5	≤ 18.5	≤ 17.5
pe	1	28	7	9	-	42.9	-	-
fd	5	158	16	54	3	38.0	76.9	-
pw	5	111	23	53	6	60.2	64.9	-
pl	18	748+61	62	353+61	9+17	55.4*	71.9	81.5

self-explanatory. RA, DEC and b_J are from the EDSGC, and velocities are in km s^{-1}. The total number of newly observed radial velocities which were accepted according to the above given criteria is 602, including 494 galaxies and 108 stars. However, due to a mismatch between the fibre and spectral numbers, seven spectra in the PL region do not have a certain identification (and thus RA and DEC), and are excluded from the tables. In Table 4(e) we have also listed the redshifts for those galaxies within the PL region which already had an (unpublished) measurement found in previous observations by one of us (MT). These are reported here for completeness, since they were not re-observed in the present survey, and will be referred to in the following as the MT sample. Earlier, less precise coordinates for these objects (originally selected from deep ESO 3.6-m telescope prime-focus plates), were matched to the EDSGC, and when possible a more precise position has been found, together with the corresponding b_J magnitude. Galaxies which did not appear in the EDSGC are indicated; no magnitude is given for these objects. The redshift errors for these external data are <100 km s^{-1}, thus comparable to those of the new data. Details will be presented in a parallel paper which concentrates on the K44 region (Ettori et al., in preparation).

The completeness of the data, defined at the given magnitude limit as the ratio of the number of galaxies with measured redshift over the total number of EDSGC galaxies, is shown in Table 5. The numbers quoted have been cleaned from those objects which were shown to be stars by the spectroscopy, and were thus deleted from the parent galaxy catalogue. For the PL region, the total sample selected from the EDSGC (809 galaxies), is explicitly split into the number of objects considered for the present survey (748) plus those from previous observations (61).

The redshifts listed as no EDSGC pertain to objects which: (i) have been serendipitously observed through one of the 'sky' fibres, on positions where no EDSGC (or previously visually identified) galaxy is present; (ii) (only for PL) are part of the MT sample, which was selected visually from deep ESO 3.6-m telescope prime-focus plates, and are missing from the EDSGC (17 objects overall in the PL region).

In general, the incompleteness is mostly due to objects which produced a too low S/N spectrum, i.e. either had too low a surface brightness or were observed through a bad fibre or in bad weather/seeing conditions. Very few objects, in fact, were not actually observed. Note also that, since the sample was selected from an early, unofficial version of the EDSGC, after the final photometric recalibration the actual magnitude limit of the PL region turned out to be $b_J = 19.62$ and not 19.5. Therefore, in Table 5 the global completeness for PL5 is referred to this slightly fainter limit, this anomaly being indicated by the asterisk in the column of the ≤ 19.5 completeness. The effects of the incompleteness on the specific analyses which have been carried out on the present data are discussed in more detail in the relevant papers.

It is interesting to plot the distribution of the R parameter and of the velocity errors ε among the whole set of measurements. These are shown in Fig. 5, and give an indication of the overall quality of the redshifts. Fig. 5(a) is constructed using the whole set of measurements, i.e. also including those spectra that were not good enough to pro-

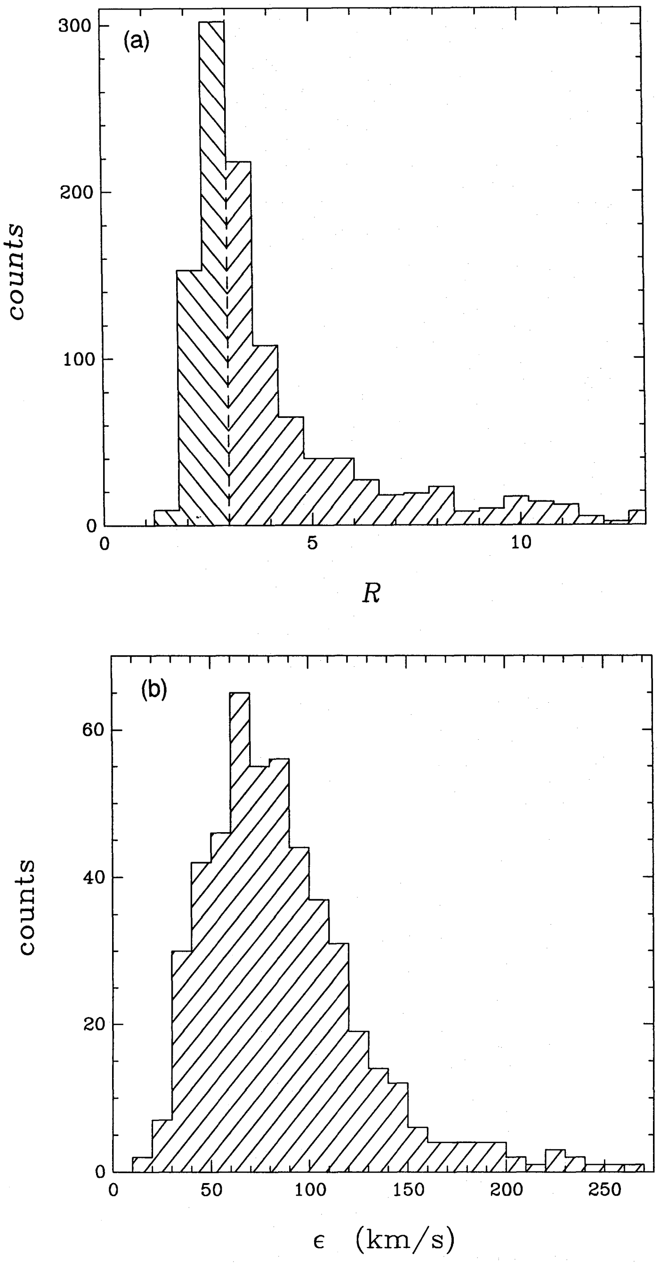

Figure 5. (a) Distribution of the value of the confidence parameter R among the whole set of measurements (including also those spectra that did not produce a significant redshift). The dashed line shows the value of the threshold in R which has been chosen as the gross borderline below which redshifts are generally discarded. (b) Distribution of the RVSAO errors ε for the selected spectra (i.e. with $R>3$); the median value of ε is ~ 75 km s^{-1}.

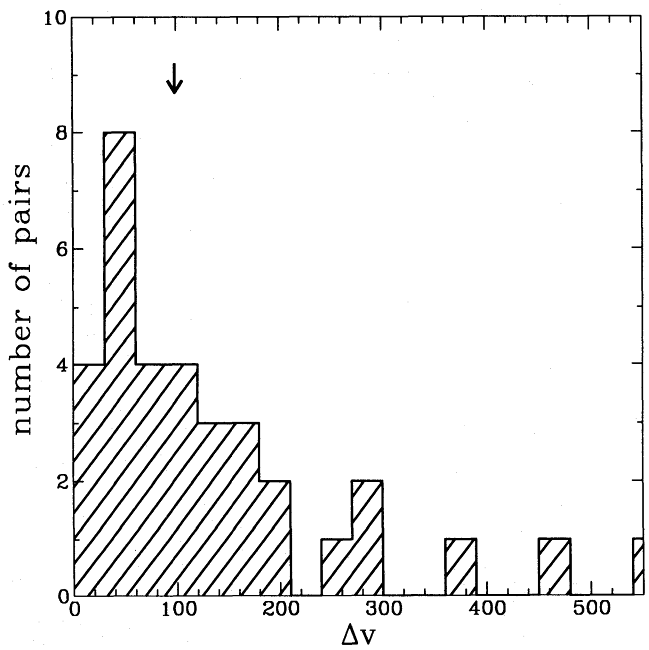

Figure 6. Distribution of the absolute differences between repeated observations of the same galaxy. The median of the distribution is 100 km s^{-1} (arrow), i.e. about 1.5 times that obtained from the internal estimate of Fig. 5(b).

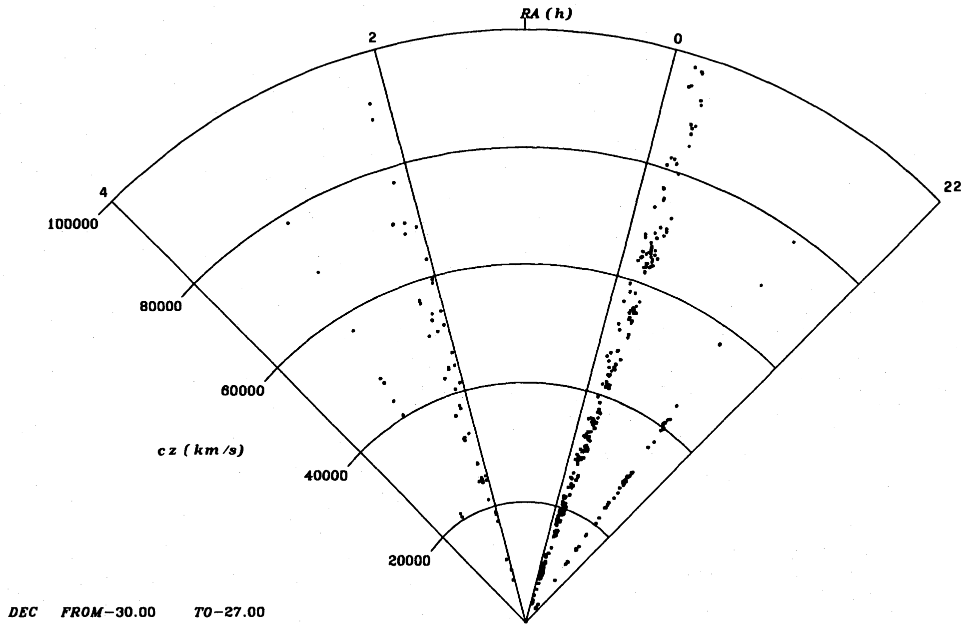

Figure 7. Right ascension wedge diagram showing the global distribution of the galaxies along the directions surveyed.

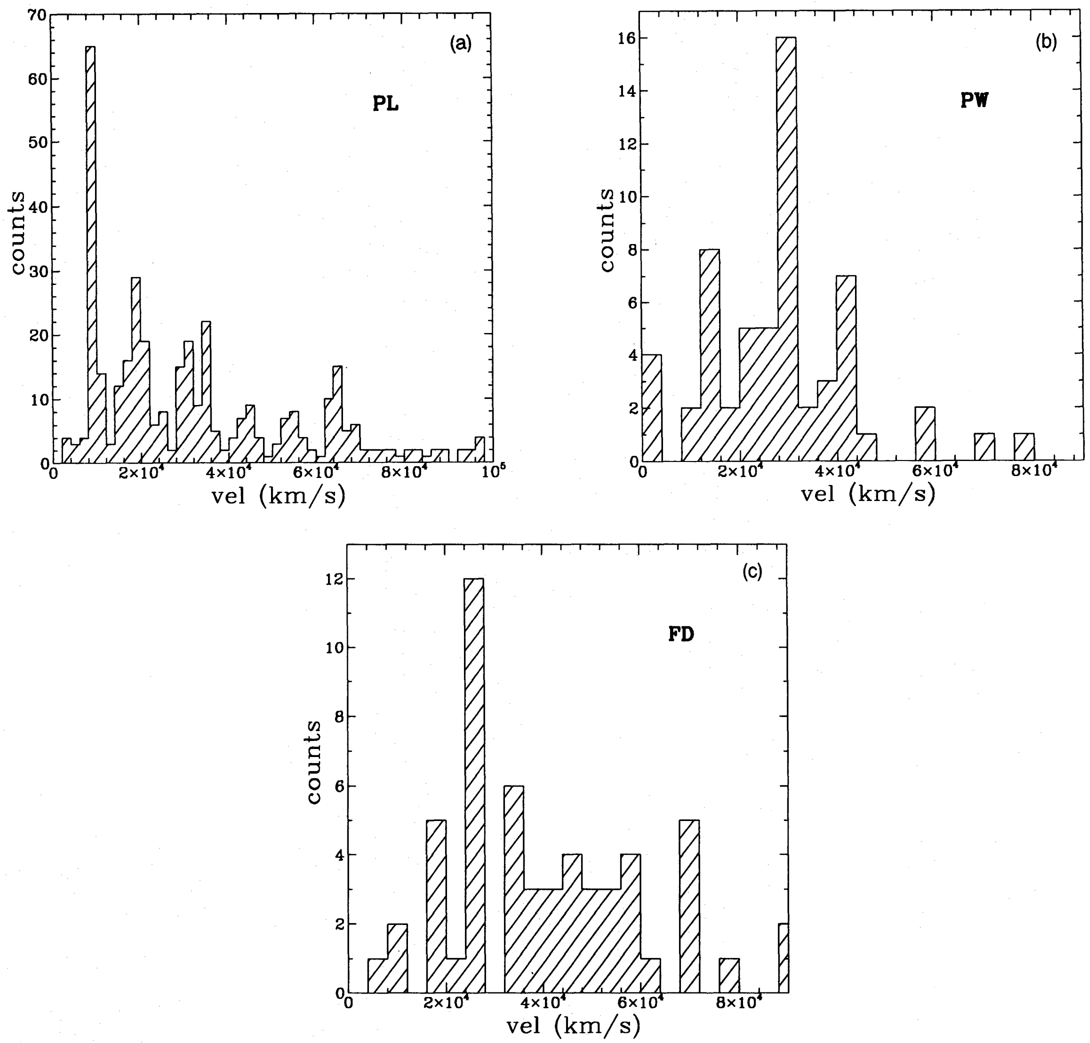

Figure 8. (a, b and c) Redshift distribution along the three main directions explored in our study. A tendency to some regularity in the spacing among the peaks of the histogram seems to be evident in the cases of PL and PW.

duce a significant estimate of the redshift. The histogram is divided into two parts by the dashed line showing the value of R chosen as the borderline below which redshifts were generally discarded. Fig. 5(b) gives the distribution of the RVSAO errors ε for those estimates with $R > 3$, showing how the median value of ε for the data presented here is ~ 75 km s^{-1}.

The error, ε, provided by the cross-correlation package, is an internal error, and is estimated on the basis of some assumptions which have been recently criticized by Heavens (1993), who proposed an alternative method for constructing a more significant error estimate. The algorithm we used is based on the original definition by TD79. We can obtain an independent estimate of the external errors by using those galaxies for which two independent observations were obtained in the survey. We have 36 pairs for which both spectra provided an acceptable redshift. In Fig. 6 we plot the distribution of the absolute differences of the two values. The median of this distribution is 100 km s^{-1}, indicated by the arrow, i.e. about 1.5 times that obtained from the internal estimate of Fig. 5(b).

A pictorial representation of the large-scale distribution along the observed beams is given in Figs 7 and 8. Fig. 7 shows a global wedge diagram of the data, while in Fig. 8 we plot the histograms of the redshift distribution in the observed fields (PE is excluded). In PL, note the expected concentration of galaxies around K44 ($cz_{K44} \sim 9000$ km s^{-1}), but also an indication for further peaks with $\sim 100\ h^{-1}$ Mpc separation. The same suggestion seems to arise when examining PW.

These qualitative considerations will be extended with a more quantitative analysis of the possible presence of a preferred clustering scale, as suggested by BEKS, in a forthcoming paper (Ettori et al., in preparation).

ACKNOWLEDGMENTS

We are indebted to G. Avila for the clever design of the upgraded version of OPTOPUS and for his help during the starplate preparation and the observations. This effort would have not been possible without the generous contribution of C. A. Collins, who provided us with galaxy positions and magnitudes from the EDSGC in advance of publication, and the help of N. Heydon-Dumbleton. Their never ending enthusiasm and patience is gratefully acknowledged. We thank G. Chincarini for many useful discussions, A. Connelly for providing us with the HD templates and R. Merighi for his help on the use of the cross-correlation package RVSAO.

REFERENCES

Avila G., D'Odorico S., Tarenghi M., Guzzo L., 1989, The Messenger, 55, 62
Beard S. M., MacGillivray H. M., Thanisch P. F., 1990, MNRAS, 247, 311
Broadhurst T. J., Ellis R. S., Shanks T., 1988, MNRAS, 235, 827
Broadhurst T. J., Ellis R. S., Koo D. C., Szalay A. S., 1990, Nat, 343, 726 (BEKS)
Collins C. A., Guzzo L., Nichol R. C., Lumsden S. L., 1995, MNRAS, 274, 1071
Ellis R. S., Parry I. R., 1988, in Robinson L., ed., Instrumentation for Ground Based Optical Astronomy. Springer, New York, p. 192
Ellis R. S., Gray P. M., Carter D., Godwin J., 1984, MNRAS, 206, 285
Geller M. J., Huchra J. P., 1989, Science, 246, 897
Giovanelli R., Haynes M. P., 1991, ARA&A, 29, 499
Giovanelli R., Haynes M. P., Chincarini G., 1986, ApJ, 300, 77
Gray P. M., 1984, in Boksenberg, A., Crawford D. L., eds, Proc. SPIE Instrumentation in Astronomy, V, 445, p. 57
Guzzo L., Tarenghi M., 1987, ESO Internal Report, 1987 October
Heavens A F., 1993, MNRAS, 263, 735
Heydon-Dumbleton N. H., Collins C. A., MacGillivray H. T., 1989, MNRAS, 238, 379
Hill J. M., 1988, in Barden S. C., ed., Fiber Optics in Astronomy, PASP, San Francisco, p. 77
Huchra J., Davis M., Latham D., Tonry J., 1983, ApJ, 52, 89
Klemola A. R., 1969, ApJ, 74, 80
Lund G., Enard D., 1984, in Boksenberg, A., Crawford D. L., eds, Proc. SPIE Instrumentation in Astronomy, V, 445, p. 65
Maddox S. J., Efstathiou G. P., Sutherland W., 1990, MNRAS, 246, 433
Oort J. H., 1983, ARA&A, 21, 373
Rood H. J., 1988, ARA&A, 26, 245
Tonry J., Davis M., 1979, AJ, 84, 1511 (TD79)
Vettolani G., 1994, in Böhringer, H., Schindler S., eds, Studying the Universe with Clusters of Galaxies. MPE report number 256, Garching, p. 7
Zwicky F., Herzog E., Karpowicz M., Kowal C. T., Wild P., eds, 1963-68, Catalogue of Galaxies and Clusters of Galaxies. Cal. Inst. Technol., Pasadena